Desalination and Water Treatment
www.deswater.com

doi:10.5004/dwt.2017.20701

73 (2017) 399–408
April

Fabrication and evaluation of activated carbon/Fe_2O_3 nano-composite on the removal of strontium ions from water

Ahmad Kayvani Fard[a,b], Gordon Mckay[b], Hugues Preud'Homme[a], Viktor Kochkodan[a], Muataz A. Atieh[a,b,*]

[a]*Qatar Environment and Energy Research Institute, Hamad Bin Khalifa University, Qatar Foundation, PO Box 5825, Doha, Qatar, email: afard@qf.org.qa (A.K. Fard), hhomme@hbku.edu.qa (H. Homme), vkochkodan@hbku.edu.qa (V. Kochkodan)*
[b]*College of Science and Engineering, Hamad Bin Khalifa University, Qatar Foundation, PO Box 5825, Doha, Qatar, email: gmckay@hbku.edu.qa (G. Mckay), Tel. +974-33199499, email: mhussien@hbku.edu.qa (M.A. Atieh)*

Received 30 June 2016; Accepted 10 March 2017

ABSTRACT

This work presents the characterization and application of activated carbon (AC) impregnated with different loadings of Fe_2O_3 nanoparticles for strontium removal from produced water. The initial strontium concentration, the strontium removal efficiency in aqueous media and the kinetics of strontium removal were analyzed by inductively coupled plasma mass spectrometer (ICP-MS). The characterization was performed using field emission scanning electron microscopy (FE-SEM) and Brunauer–Emmett–Teller (BET) surface analysis. Different experimental parameters such as adsorbent dosage, pH of the solution, agitation speed and contact time, were investigated for their effects on the adsorption of strontium from water. The optimum condition for maximum removal of the solute was observed to be 150 min of contact time with the sorbent, pH 7, 150 mg adsorbent dosage and 400 rpm rotational speed. Also it was observed that surface modification of AC with Fe_2O_3 nanoparticles enhanced their adsorption efficiency. AC loaded with 1% Fe_2O_3 could remove 93% of strontium while when the nanoparticles loading increased to 10%, the solute was completely removed from water. The results obtained are promising for the use of AC loaded with Fe_2O_3 nanoparticles in the pretreatment of produced water before the desalination process. Adsorption can be very efficient with low energy consumption and economic feasibility.

Keywords: Adsorption; Strontium; Desalination; Pre-treatment; Water treatment; Seawater

1. Introduction

Oil and natural gas play a significant role in our modern civilization. The rapid economic growth in parallel to the high demand for oil and gas attributed to the general fact that oil and gas are the primary source of energy and building block for many of the substances such as polymers, petrochemicals fuels, and many more products [1]. On the other hand, like other industrial activities, Currently oil and gas industries generate large volumes of liquid waste [1]. The volume of produced water from oil/gas fields is estimated to be around 250 million barrels per day compared with around 80 million barrels per day of oil [2]. This is equivalent to around 3 barrels of produced water per each barrel of water produced. Oil field wastewater or produced water contains many organic and inorganic components [3]. Factors such as geological location of the oil/gas field, well's lifetime, and type of hydrocarbon product being extracted from the field have a direct relation to the physical and chemical composition of produced water [4]. Produced water generally consists of: dissolved and dispersed oil compounds, dissolved formation minerals, production chemical compounds (inhibitors for preventing scaling and corrosion), bacteria, waxes, asphaltenes, and dissolved gases [5]. The total dissolved solid (TDS) concentration in produced water may reach 300,000 ppm in many fields. The TDS include anions (Cl^-, SO_4^{2-}, CO_3^{2-}, HCO_3^-), cations (Na^+,

*Corresponding author.

Presented at the EDS conference on Desalination for the Environment: Clean Water and Energy, Rome, Italy, 22–26 May 2016.

K^+, Ca^{2+}, Mg^{2+}, Ba^{2+}, Sr^{2+}, Fe^{2+}), heavy metals (cadmium, chromium, copper, lead, mercury, nickel, silver, zinc) and radioactive materials. One of the elements of special concern is strontium. Strontium (Sr^{2+}) is alkaline earth metal and it is the 15th most abundant element in earth crust with average concentration of 0.04 wt.%. Although strontium is chemically stable, its isotopes are considered radioactive. In sea water and co-produced water, strontium is considered as the 10th most available element with concentrations reaching up to 590 ppm [2].

In the human body, strontium can replace calcium due to its chemical and structural similarities. The radioactive ^{90}Sr can lead to various bone disorders and diseases, including bone cancer. Therefore it is very essential to remove strontium from produced water before dumping it to the sea. This is especially important for areas where seawater is the primary source for drinking water through seawater desalination.

Different methods for the removal of strontium from water is reported in literature such as chemical precipitation [6], ion exchange [7], adsorption [8,9], and membrane separation [10–12]. One of the feasible, and most effective techniques used in industries is the adsorption process. Different types of adsorbent materials are suggested for strontium removal such as activated carbon (AC) [13], pecan shells [14], montmorilonite and zeolite [15], eggplant hull [16], manganese dioxide [17], clay minerals [18], sawdust [19], goethite [20], hematite [21], bentonite [22], and kaolinite [23].

The combination of a high surface area of AC with magnetic properties of iron-oxide nanoparticles is attractive for the preparation of a novel adsorbent for strontium removal.

For the first time, in this study we reported the synthesis of doped AC with Fe_2O_3 nanoparticles and their application for the removal of strontium from water. Commercial AC with different loadings of Fe_2O_3 nanoparticle were prepared and effect of pH, adsorbent dosage, sorption kinetic are studied and the optimum conditions for the removal of Sr^{2+} from water are reported. The prepared composite sorbent is characterized by field emission scanning electron microscopy (FE-SEM), powder X-ray diffraction (XRD), Thermogravemetric analysis (TGA), and the Brunauer, Emmett and Teller (BET) nitrogen adsorption technique.

2. Materials and methods

2.1. Material

The AC with particles size of 0.60–1.0 mm used in this study was purchased from Calgon Carbon (China). Ethanol (98%, purity) as a solvent, ferric nitrate ($Fe(NO_3)_3{\cdot}9H_2O$ (99 % purity), as a precursor of the iron nanoparticles, and the strontium standard solution with concentration of 1000 mg/L were obtained from Sigma-Aldrich. All the chemicals were used without further purification.

2.2. Preparation of AC-Fe_2O_3 composite

The loading of Fe_2O_3 nanoparticles on the AC surface was carried out using the wet impregnation method found elsewhere [3]. Briefly, a fixed amount of ferric nitrate based on the required ratio of Fe_2O_3 nanoparticle loading was dissolved in 500 ml of ethanol containing a fixed amount of AC. AC with 1% and 10% loadings of iron oxide nanoparticles were prepared by changing the concentration of ferric nitrate in aqueous ethanol solutions. The solutions were sonicated for 45 min to disperse the iron precursor and AC homogeneously. The aqueous solution is then evaporated at 70°C in an oven. The residue was calcined at 350°C for 4 h in an oven in the presence of air to prepare the iron oxide nanoparticles from iron nitrate.

2.3. Strontium and trace element analysis

Initial and final concentrations of strontium were measured using a Brucker Aurora Elite inductive coupled plasma-mass spectrophotometer (ICP-MS). Samples taken at different time are dosed, preserved and diluted 100 times with 1% HNO_3/H_2O prior to the testing. The elemental strontium (^{86}Sr, ^{87}Sr & ^{88}Sr) and trace elements such as carbon (^{13}C), chromium (^{52}Cr and ^{53}Cr), iron (^{54}Fe, ^{57}Fe) in helium collision mode (67 ml/min.) were analyzed with an ICPMS CRI2 Aurora Elite, ICP-MS from Bruker Daltonics using a dwell time of 30 ms, 10 replicates and a plasma power of 1450 W.

2.4. AC/Fe_2O_3 characterization

The morphologies of the AC/Fe_2O_3 composites as well as elemental analysis (EDX) were analyzed with a TESCAN MIRA 3 FEG-SEM, field emission scanning electron microscope using an acceleration voltage of 20 kV. The surface areas of the AC/Fe_2O_3 composites were measured by N_2 adsorption at 77 K using a BET surface area analyzer Micromeritics ASAP 2020. XRD patterns were recorded using a Rigaku MiniFlex-600 X-Ray diffractometer with Cu Kα radiation λ = 1.54Å at a rate of 0.4% over Bragg angles ranging from 10–90 degrees. The operating voltage and current were maintained at 40 kV and 15 mA, respectively. For physical and chemical property analysis of the AC nanocomposite with respect to temperature, thermogravimetric analysis (TGA) (SDT, Q600, TA Instruments) at a heating rate of 10°C/min in air was used. Prior to any analysis, the TGA analyzer was calibrated for temperature readings and mass changes using a nickel reference material.

2.5. Batch experiments

Batch experimental mode was used to study effect of adsorbent dosage, pH, and contact time on the removal efficiency and adsorption capacity of AC/Fe_2O_3 composite. The adsorption capacity (Q) and removal efficiency (RE) were calculated as follows:

$$Q = \frac{\left(C_i - C_f\right) \times V}{W_g} \tag{1}$$

$$RE(\%) = \frac{\left(C_i - C_f\right)}{C_i} \times 100 \tag{2}$$

where C_i (mg/L) is the initial concentration of strontium in the water, C_f (mg/L) is the final concentration of the remain-

ing strontium in the water, V (L) is the volume of the water, and W_g is the mass of adsorbent.

All the batch experiments were performed by adding 20 mL of solution containing specific concentrations of strontium to specific amount of the AC composite. All the experiments were performed at room temperature. The effect of the strontium concentrations on the adsorption capacity and removal efficiency was tested by varying the initial strontium concentrations from 0.5 ppm (mg/L) to 50 ppm. The equilibrium studies were carried out for 150 min to determine the equilibrium contact time and adsorption capacity. To find the optimum amount of adsorbent dosages for maximum removal of strontium from water, different weights of AC/Fe_2O_3 varied from 5 to 150 mg was used. All the samples were agitated using a mechanical shaker at 400 rpm.

A standard stock solution of strontium with concentration of 1000 mg/L was used for the preparation of Sr(II) solutions of different concentrations. The pH of the solutions were adjusted with 0.1 M HCl and 0.1 M NaOH to study the effect of pH on adsorption capacity and Sr (II) removal with AC/Fe_2O_3.

2.6. Preparing the stock solution

Solutions of different concentration of strontium were prepared for the analysis. Initially, all the glass wares were washed with 2% nitric acid and ethanol to remove all the impurities and avoid any further adsorption of dust or particles in the air. A standard solution of strontium with concentration of 1000 mg/L was used to produce the stock solutions. A specific volume of Sr(II) was added to a 2 L volumetric flask and ultra-pure deionized water was added to reach a total volume of 2 L to fully mix the solutions, a magnetic stirrer was used. To adjust the pH 0.1 M NaOH and 0.1 M HCl were used. A constant pH was maintained by the addition of buffer solution.

2.7. Adsorption isotherms

The adsorption energy and maximum adsorption capacity of AC/Fe_2O_3 for removal of strontium were calculated using Freundlich, Langmuir, and Dubinin–Radushkevich (D–R) isotherm models. The mathematical equation for Freundlich isotherm can be expressed as:

$$Q_e = K_F C_e^{\frac{1}{n}} \tag{3}$$

where Q_e is the adsorption capacity at equilibrium, C_e is the strontium concentration at equilibrium (mg/L), and n and K_F are Freundlich empirical constants that indicate the sorption intensity and the sorption capacity of the adsorbent, respectively. The Freundlich model assumes a heterogeneous adsorbent surface and energy distribution for the different sites. A linearized form of the Freundlich isotherm can be expressed as:

$$\ln Q_e = \ln K_F + \frac{1}{n}\ln C_e \tag{4}$$

On the other hand, the Langmuir isotherm model assumes that adsorption takes place at defined homogeneous sites on adsorbent surface. This means that the Langumir model supports a monolayer adsorption phenomena in comparison to the Freundlich model which supports a multi-layer adsorption concept. This means that once a strontium ion occupies a site on the surface of AC/Fe_2O_3, no further strontium ions could adsorb on that site. The Langmuir isotherm is expressed as:

$$Q_e = \frac{X_m K C_e}{(1 + K C_e)} \tag{5}$$

where K is the Langmuir constant, and X_m is the maximum adsorption capacity (mg/g).

The linearized form of the Langmuir isotherm can be rearranged and expressed as:

$$\frac{C_e}{Q_e} = \frac{1}{X_m K} + \frac{C_e}{X_m} \tag{6}$$

The Langmuir constants K and X_m, which are related to the constant free energy of sorption, can be determined by representing a linear plot of C_e/Q_e vs. C_e from the intercept and slope of the plot.

To estimate the adsorption mechanism with a Gaussian energy distribution onto a heterogeneous surface, the data is modeled to the Dubinin–Radushkevich (D-R) isotherm model [24]. The linear form of the model is:

$$\ln Q_e = \ln Q_m - (2B\varepsilon) \tag{7}$$

where B is the Dubinin–Radushkevich isotherm constant (mol²/kJ²) and ε is Dubinin–Radushkevich isotherm constant and expanded as:

$$\varepsilon = R\,T \ln\left(1 + \frac{1}{C_e}\right) \tag{8}$$

A plot of $ln\ Q_e$ vs. ε enables the determination of isotherm constants B and Q_m from the slope and intercept. The mean free energy denoted as E per strontium ion adsorbed is then calculated [25]:

$$E_a = \frac{1}{\sqrt{2B}} \tag{9}$$

The E (kJ/mol) value represents evidence about the type of adsorption mechanism. If the value of free energy is between 8 and 16 kJ/mol, the adsorption process occurs by chemical ion-exchange, while for E < 8 kJ/mol, the adsorption process proceeds physically, and when an E value is higher than 16 kJ/mol, the adsorption process is chemisorption in nature [26].

2.8. Adsorption kinetics

The aqueous solution (20 ml) mixed with 150 mg of AC/Fe_2O_3 composites were agitated at 400 rpm using a mechanical shaker at 25°C. Different samples were taken from the solution at specific time intervals and after being filtered and centrifuged at a speed of 13000 rpm for 5 min, Sr (II) concentration in the samples was measured using ICP-MS analyzer.

In order to find the time for a maximum strontium uptake by AC/$Fe_2O_3$and to evaluate the rate of reaction, two kinetic models namely, pseudo-first-order and pseudo-second-order were employed to model the data.

The Lagergren pseudo-first-order model states that the rate of adsorption of adsorbate on adsorbent is proportional to the number of sites unoccupied by the adsorbate [27]. The pseudo-first-order equation can be written in a linearized form as follows:

$$\ln\left(Q_e - Q_t\right) = \ln Q_e - k_1 t \tag{10}$$

where q_t is the sorption capacity (mg/g) at any present time interval (t) and k_1 is the first-order rate constant (min^{-1}), which can be found from a linearized graph of $\ln(Q_e - Q_t)$ vs. time.

Additionally, the adsorption data were analyzed using the pseudo-second-order kinetic model [28]. The linear form of the pseudo-second-order kinetic model can be written ina linearized form as:

$$\frac{t}{Q_t} = \frac{1}{k_2 Q_e^2} + \frac{t}{Q_e} \tag{11}$$

where k_2 is the second-order rate constant (g/mg·min), which can be found by plotting t/Q_t vs. time.

3. Results and discussion

3.1. Characterization of AC doped with Fe_2O_3 nanoparticles

The surface morphologies of the activated carbon and AC/Fe_2O_3 composite adsorbents were observed using FE-SEM. Fig. 1 shows the SEM images of commercial AC and AC with 1 wt.% Fe_2O_3 and 10 wt.% Fe_2O_3 nanoparticles. From Fig. 1, the size of nanoparticles appeared to be in range of 1–10 μm. It can be observed that, when the Fe_2O_3 loading is increased, nanoparticles tend to agglomerate and form the clusters as can be seen in Fig. 1b. No major changes on the surfaces of doped AC can be seen after calcination and impregnating with Fe_2O_3 nanoparticles.

To confirm the presence of iron and also to investigate the exact amount of iron oxide nanoparticles on the surface of AC, SEM-EDX and elemental mapping have been carried out and the results are summarized in Table 1 and Fig. 2, respectively.

The EDX analysis of the raw AC and composite AC with Fe_2O_3 NP, which represents the atomic weight percentage (%) of the elements such as Fe, O and C, are shown in Table 1. The Fe/C ratios extracted from the EDX are close to the experimental values for the prepared samples.

In Fig. 2, we present the elemental mapping for raw AC and AC with different percentage of iron oxide nanoparticles. The relative concentrations of each element in Fig. 2 are represented by the color scale, as it is obtained from scaling the hue according to the minimum and maximum X-ray intensity. The SEM-EDX mapping inside the selected region confirms the existence of Fe_2O_3 NPs in the high ntensity zones correlated to the Fe oxide NPs. On the other hand, Fig. 2 shows very well the distribution of O or O-containing groups on the carbon surface, which also, can be seen with the Fe which is another indication of the presence of Fe oxide NPs. The results confirm that very small iron oxide NPs are formed on the surface of AC by the wet impregnation method and the NPs are very well and homogeneously distributed through the AC pore network.

Fig. 3 shows the XRD patterns of raw AC and AC samples with different ratios of Fe_2O_3 nanoparticles. The AC peaks for raw AC and AC with 1 and 10% Fe_2O_3 loading are indicated at 2θ of 24° and 43°, which correspond to 002 and

Table 1
EDX analysis of raw AC and AC with different percentage of α-Fe_2O_3

CNT Sample	Raw AC	AC- 1% Fe_2O_3	AC- 10% Fe_2O_3
Element	Weight %	Weight %	Weight %
C	88.34	76.13	55.74
O	11.66	21.96	33.00
Fe	0	1.91	10.27
Total %	100	100	100

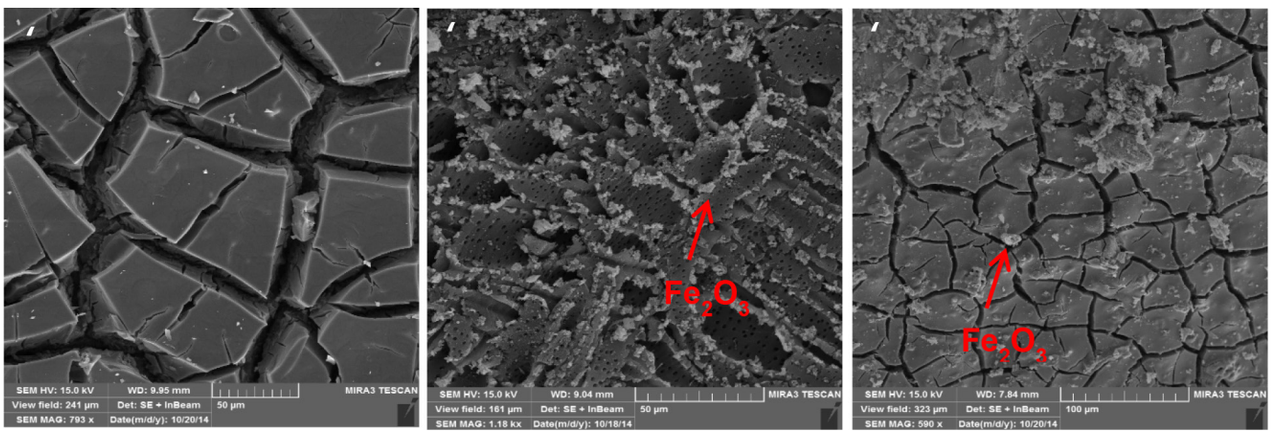

Fig. 1. SEM image of commercial AC (a) and AC with 1% Fe_2O_3 nanoparticle loading (b) and 10% Fe_2O_3 nanoparticle loading (c).

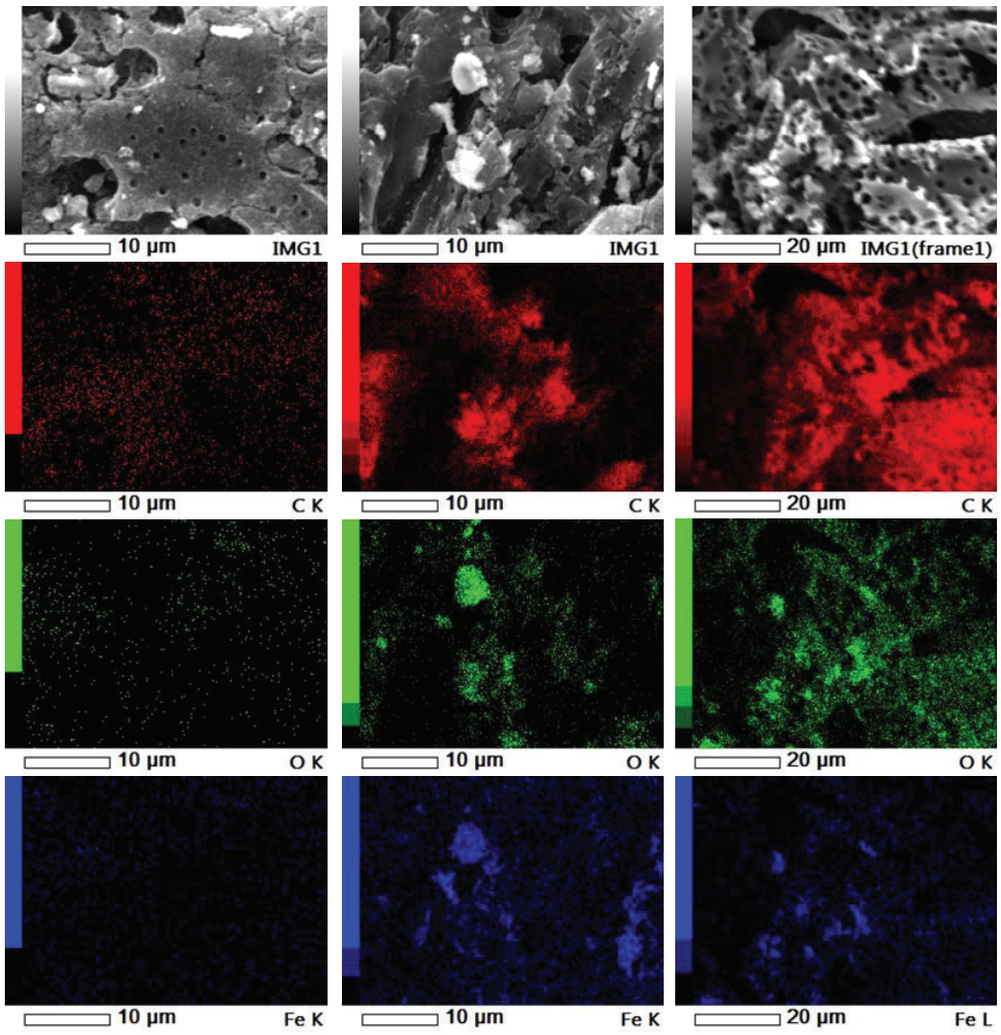

Fig. 2. EDX elemental mapping of Raw AC (a) and AC with 1% (b) and 10% (c) Fe_2O_3 nanoparticle loading.

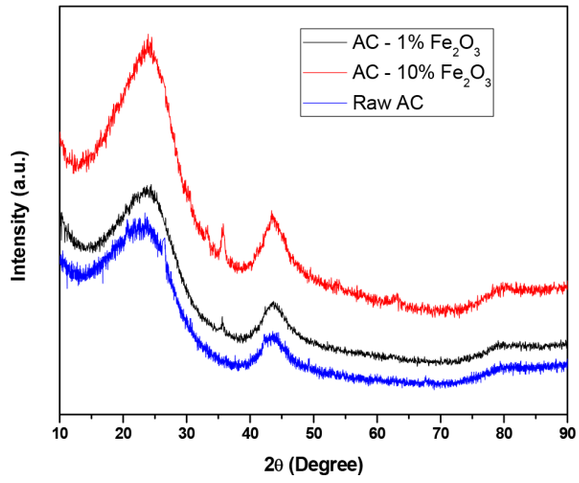

Fig. 3. XRD patterns of AC/Fe_2O_3 composite with 1 wt.% and 10 wt.% loading.

100 planes, respectively. The XRD peaks of AC are a typical diffraction pattern of an amorphous material with not well defined resolved peaks and broad peaks.

The two samples with 1 and 10% Fe_2O_3 loading in addition to the AC peaks, also showed the presence of Fe_2O_3 crystal as the distinct peak at 2θ of 33° which corresponds to 220 plane. There is another peak at 2θ of 24° which corresponds to the101 plane but the peak added up to the peak of AC. Therefore, the peak at 2θ of 24° is broad and has a slight shift to lower degree.

The BET surface areas of commercial AC and AC with 1 wt.% and 10 wt.% loading of Fe_2O_3 were found to be 1126 m^2/g, 1271 m^2/g, and 1309 m^2/g, respectively. The adsorption isotherms with N_2 at 77 K are shown in Fig. 4. Impregnating the surface of AC with Fe_2O_3 nanoparticle enhanced the surface area of AC and this will increase the number of adsorption sites which will enhance strontium ions removal by AC.

Thermogravimetric analysis (TGA), Simultaneous Difference Thermal Analysis(SDTA), and derivative thermogravimetric analysis (DTGA) were used to determine the

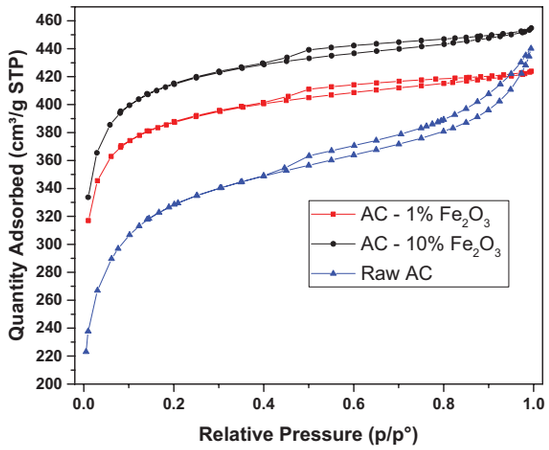

Fig. 4. BET adsorption isotherm with N_2 at 77 K for AC/Fe_2O_3 composite with 1 wt.% and 10 wt.% loading.

thermal stability, the purity of the non-modified and modified adsorbents, and the percentage of iron oxide nanoparticles on the surface of modified AC. The thermal analyses are shown in Fig. 5. The analysis was performed under air at a heating rate of 10°C/min up to 850°C.

In all the three cases in Fig. 4, the sample mass decreases slightly at the beginning of the measurement at temperatures lower than 100°C. This effect is related to residual moisture and other volatile components in the samples and can be clearly distinguished from the decline in the mass percentage at any other temperatures. Another sharp mass decrease occurs at temperature between 350–550°C which is caused by the oxidation and decomposition of activated carbon. TGA analysis in Fig. 4 reveals that the raw AC is thermally stable and starts to decompose at around 410°C forming carbon dioxide. On the other hand modified AC impregnated with 1% and 10% iron oxide NP starts to decompose at 390°C and 407°C, respectively. This result was expected due to the presence of thermally unstable functional groups and metallic NP which acts as a heating source on the surface of AC. These NP store the heat and cause spot heating on the surface of AC. In addition to the heating rate supplied from the furnace this heating spot has fasten the decomposition and consequently makes the AC with Fe_2O_3 NP oxidize at a lower temperature compared to raw AC. The slight difference between AC with 1% Fe_2O_3 and 10% Fe_2O_3 is due to the even distribution of NP with 1% Fe_2O_3 loading compared to the aggregated NP with the 10% Fe_2O_3 loading. Even the distribution of metallic NPs on the surface of AC, causes the heat to completely cover the surface of AC and therefore oxidize the AC at lower temperature. Extra information which can be extracted from the TGA thermograms in Fig. 5a is an accurate estimate of the loading of iron oxide NPs doped on surface of AC by comparing the residues for the complete oxidation of the raw and impregnated AC samples. It can be seen from Fig. 5a, that the raw AC fully decomposed to CO_2 at temperatures above 560°C and this can be seen by the 0% residual weight at the end of the process. On the other hand, as the Fe_2O_3 content on the surface of AC increased, higher residual yields have been found which

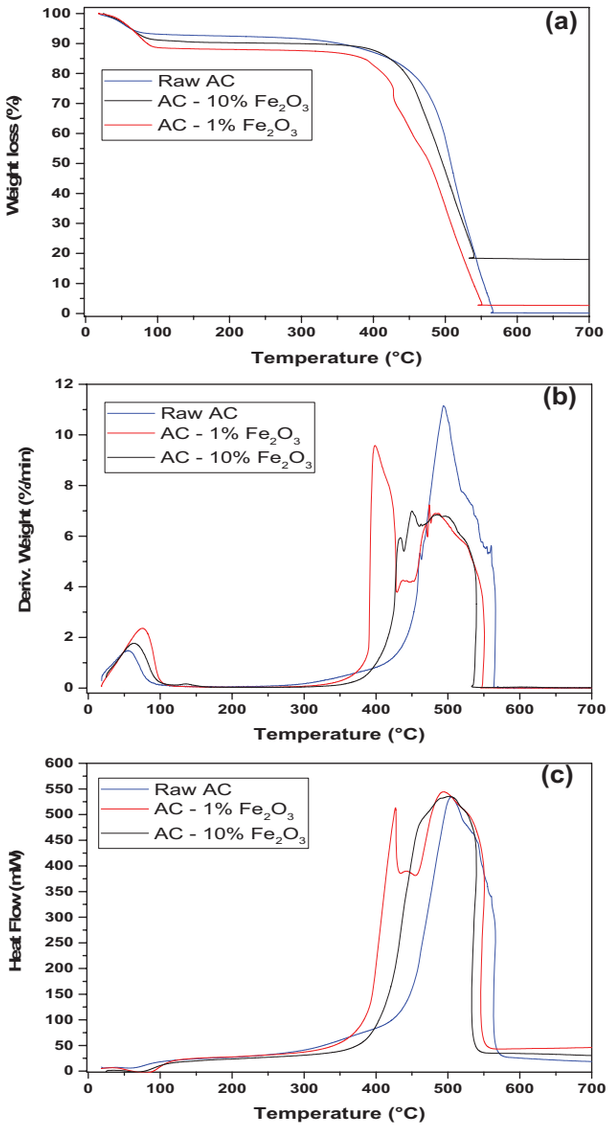

Fig. 5. TGA thermal curve (a), derevative TGA (b), and diferential scanning calorimter (DSC) (c) for raw AC and AC with 1% and 10% Fe_2O_3.

correspond to the presence of iron oxide NPs on the surface of AC. Therefore, AC with 1% and 10% Fe_2O_3 loadings have residual yields of 2.6 wt.% and 16 wt.%, respectively. The difference might be due to presence of more NP in the analyzed sample.

DTG analysis has been performed simultaneously with TGA and the thermograms are shown in Fig. 5b. For all the three cases, two broad peaks can be observed in which the first peak is attributed to the desorption of moisture and volatile compounds and the second peak is attributed to the oxidation and decomposition of AC.

The DSC curves in Fig. 5c confirm the finding of the TGA by showing an endothermic reaction for the evaporation of water and an exothermic reaction between 350–550°C for the decomposition of carbon to form CO_2.

3.2. Effect of adsorbent dosage

Different amounts of AC/Fe_2O_3 composite, ranging from 20 to 150 mg, were examined under a batch mode while fixing the pH at 7, contact time of 150 min and agitation speed of 400 rpm. The solution volume was 20 ml for all cases. Fig. 6 shows Sr (II) removal efficiency as a function of the adsorbent dosage. It can be observed that strontium removal increased with the increase in the adsorbent dosage for both 1 wt.% and 10 wt.% Fe_2O_3 nanoparticle loading. For the adsorbent dosage of 150 mg the removal was observed to be around 96% and 100% for 1 wt.% and 10 wt.% AC/ Fe_2O_3 nanocomposite, respectively.

The increase in the removal of Sr (II) ions at higher AC dosage is due to the availability of a higher number of active adsorption sites on surface of AC. The slight increase in Sr (II) removal when the loading of Fe_2O_3 nanoparticles increased to 10 wt.% is due to the further increase in surface area of nanoparticles and hence to a higher number of available adsorption sites.

3.3. Effect of pH

To study the effect of pH on the adsorption of strontium, batch experiments at different pH values were conducted at the fixed adsorbent dosage, fixed contact time, and fixed shaking speed of 150 mg, 150 min, and 400 rpm respectively. Fig. 7 shows Sr (II) removal from aqueous solutions as a function of pH at the solute concentration of 1 mg/L. It was observed that the removal of strontium increased by increasing pH where maximum removal was observed at pH 7. The adsorption reduced thereafter at the basic pH of 10. It is clear that the uptake of strontium at acidic pH is quite impressive compared to that of basic pH. The same findings were observed for both composite sorbents with different Fe_2O_3 loading. Generally, the adsorption of metal cations such as Sr (II) is usually smaller for solutions with low pH. This is due to the fact that at a low pH value there is a strong competition between the excess of hydrogenions and metal cations for the adsorption sites on AC surface, therefore reducing the available adsorption sites for strontium ions. As pH increases, the concentration of hydrogen ions in the solution reduced and hence Sr (II) removal from the solution increased[29].

Depending on solution pH, the surface of metal oxides can be negative, positive, or neutral as per following mechanism:

$$\underbrace{MOH_2^+}_{positive} \leftrightarrow \underbrace{MOH^0}_{neutral} + H^+$$

$$MOH^0 \leftrightarrow \underbrace{MO}_{negative} + H^+$$

At acidic pH, the metal oxide surfaces act as a positive character with less affinity for cations; while at higher pH values they behave as a negatively charged surface, as a result of which the uptake is a maximum at higher pH; at basic pH, metal oxide form precipitate and they don't present in bulk solution. Strontium is present as cations below pH 5 but precipitates as the negatively charged $Sr(OH)_2$ at higher pH (pH 9 and higher) as per following reaction [16,30]. According to strontium (II) hydrolysis constants, the distribution of strontium species in water at the pH values from 1 to 11 can be present in the form of Sr^{2+} and a very negligible $Sr(OH)^+$ which increases in concentration above pH above 10 and becomes the predominant species above pH 13. Therefore, at the pH range of 1–10, strontium (II) has been found to be in the form of Sr^{2+} [18].

$$Sr + 2H_2O \rightarrow Sr(OH)_2 + H_2$$

On the other hand, the surface of AC/Fe_2O_3 is positively charged and the magnitude of the surface charge is higher (more positive) at higher Fe_2O_3 loadings. Therefore at pH 7, negatively charged strontium ions adsorb more readily on surface of the positively charged AC composite. Sr adsorption is observed to be higher when Fe_2O_3 loading is increased to 10 wt.%.

3.4. Effect of contact time

The effect of contact time on strontium adsorption by AC/Fe_2O_3 composites was investigated and it was shown that an increase in contact time leads to enhanced of strontium

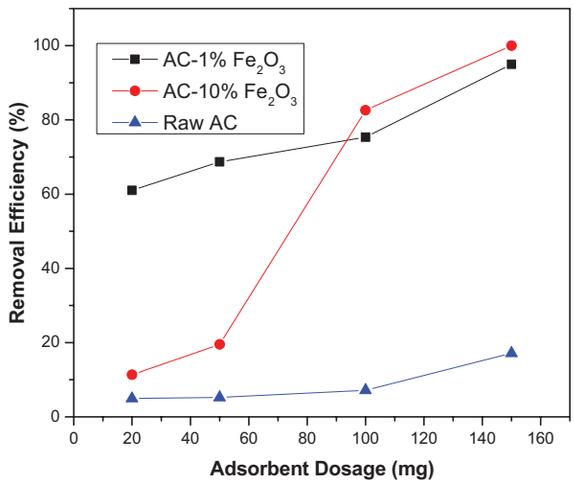

Fig. 6. Effect of adsorbent dosage on Sr (II) removal.

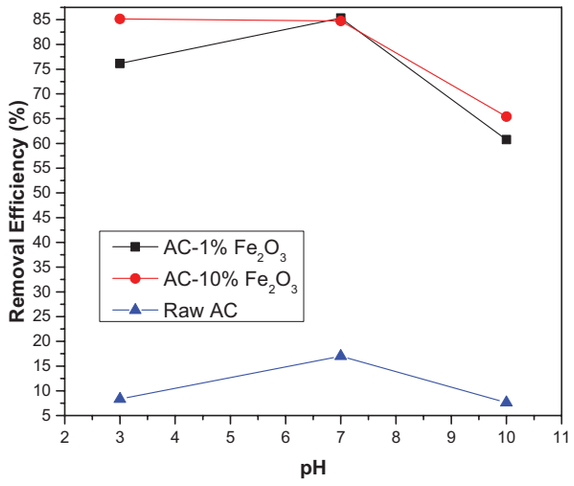

Fig. 7. Effect of pH on the removal efficiency of strontium.

removal up to the maximum equilibrium adsorption capacity. The removal efficiency of AC with 10 wt.% Fe_2O_3 nanoparticles was observed to be higher than that of 1 wt.% Fe_2O_3 indicated in Fig. 6. As shown in Fig. 8, the Sr (II) removal increases with contact time for both 1 wt.% and 10 wt.% AC/Fe_2O_3 sorbents until adsorption equilibrium was reached, where initially, the rate of adsorption was higher than the rate of desorption until 110 minutes which is the equilibrium adsorption point. At this specific time, the rate of adsorption and desorption are the same and no further Sr removal occurs. The removal of Sr (II) ion by AC loaded with 1 wt.% and 10 wt.% Fe_2O_3 nanoparticle is 90% and 100%, respectively.

Contact time is an important parameter in a batch adsorption mode as it determines the adsorption cycle duration. Shorter equilibrium adsorption times strengthens the likelihood that the adsorption is physical while longer time suggests that the adsorption is chemical.

3.5. Adsorption kinetics

The adsorption kinetics of strontium on AC/Fe_2O_3 composites was studied using the Lagergren pseudo-first order model and pseudo-second-order model. The data on strontium adsorption with AC/Fe_2O_3sorbents fits very well to the pseudo-second-order model with coefficients of determination being close to unity. The data does not show linear behavior in the first order model and therefore the system cannot be correlated to the first order kinetic model. The R^2 of the linearized plots for first order model are less than 0.9 for both cases. Fig. 9 illustrates the linearized plots of first and the second order model fitting for the strontium adsorption and constants are summarized in Table 2.

Both the calculated and experimental Q_e values for strontium adsorption were close to each other. Therefore high correlation coefficient and the good agreement of experimental and calculated Q_e values both suggested that the adsorption kinetics of strontium on AC/Fe_2O_3 followed the pseudo-second-order model. It is also shown that when percentage of loading of Fe_2O_3 increases from 1 to 10 wt.% the adsorption capacity increases by almost 10 times.

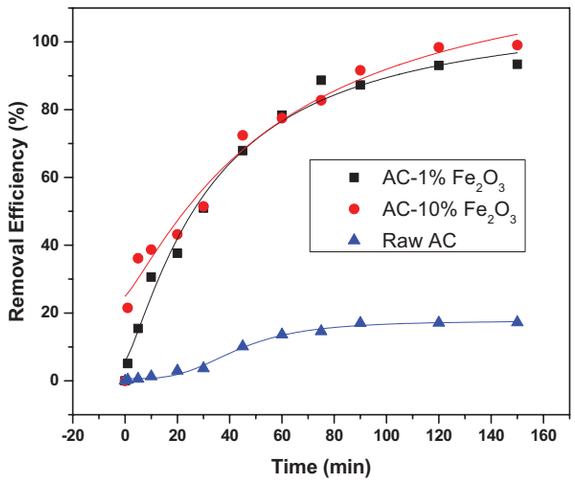

Fig. 8. Kinetic study of removal of strontium from aqueous solution.

3.6. Adsorption isotherm

The adsorption isotherm models of Langmuir, Freundlich, and D–R were applied to fit the adsorption equilibrium data of strontium on the AC/Fe_2O_3 composite with different loadings (Fig. 10). The constant values calculated for each isotherm models are listed in Table3.

Aqueous solutions with initial strontium concentrations of 0.5, 1.0, 5.0, 20, and 50.0 mgL^{-1} were used for the experiments at pH 7, adsorption time of 2 h, and temperature of 25°C.

The Freundlich constant *1/n* for 1 wt.% and 10 wt.% Fe_2O_3 loading was found to be 0.23 and 1.078, respectively. When value of $1/n > 1$ it implies that the process is a favorable which means that the strontium adsorption on AC

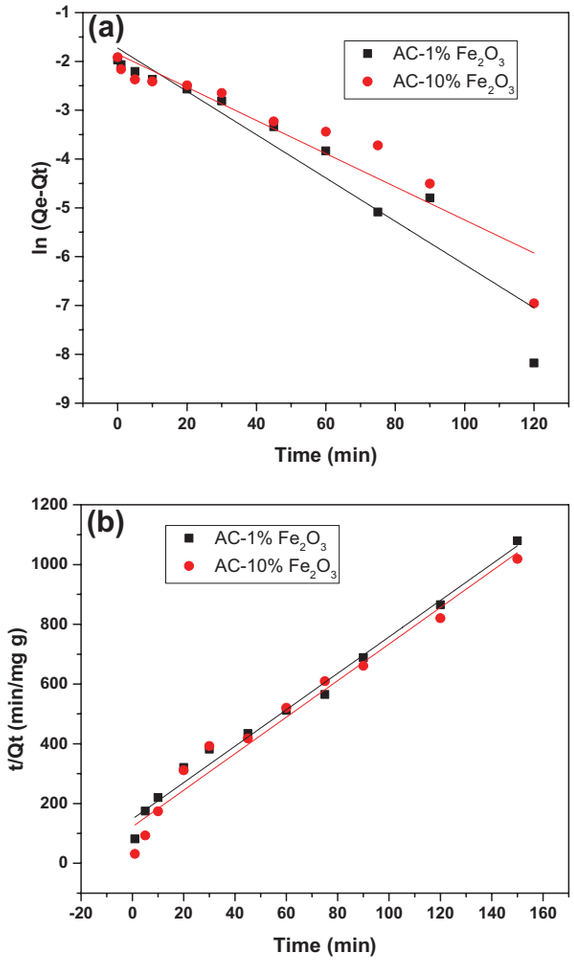

Fig. 9. Linear data fit for first order (a) and second order (b) kinetic model.

Table 2
Kinetic parameters for second order model

Sample	Q_e (mg/g)	k_2 (g/mgh)	R^2
AC/1% Fe_2O_3	0.013	–73.09	0.98
AC/10% Fe_2O_3	0.152	0.46	0.95

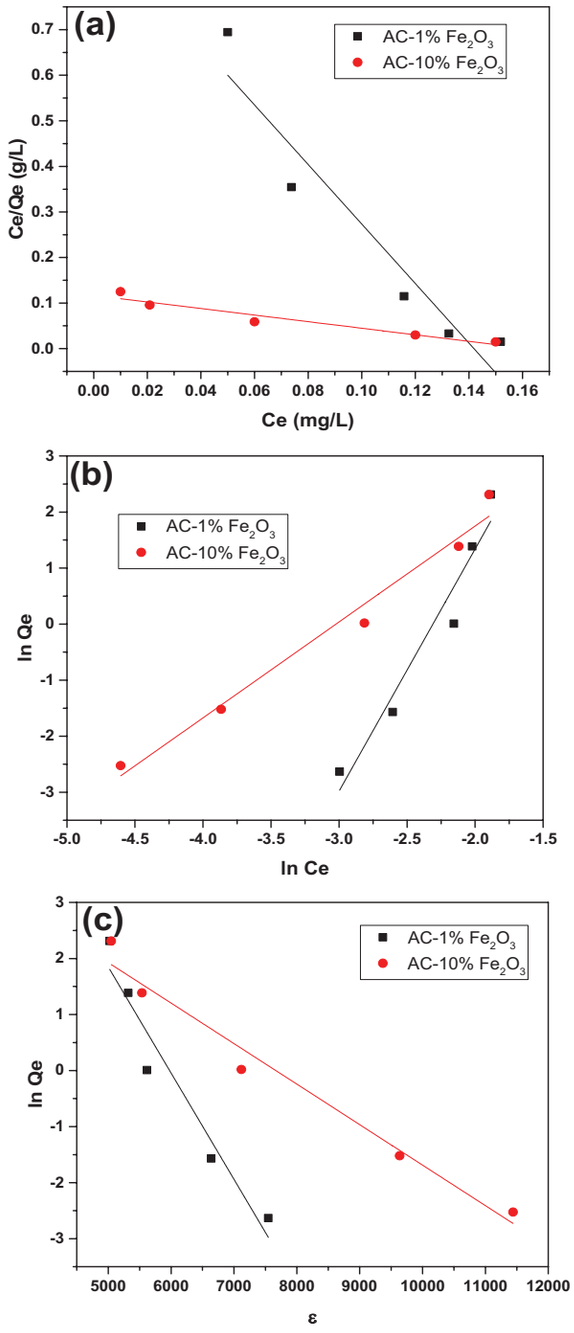

Fig. 10. Langmuir (a), Freundlich (b), and D–R (c) adsorption isotherms of strontium on AC/Fe_2O_3 composite.

with 10 wt.% Fe_2O_3 loading is more favorable compared to AC with 1 wt.% Fe_2O_3 loading. At room temperature (25°C), the Freundlich model fitted the adsorption isotherms better than the Langmuir model. This means that strontium adsorption is not restricted to the formation of a sorbate monolayer onto the heterogeneous surface of AC. Therefore, the amount of strontium adsorbed on AC is the summation of the adsorption on all sites (each having bond energy), with the stronger binding sites occupied first, until the adsorption energy exponentially decreases upon the completion of the adsorption process.

Table 3
Langmuir, Freundlich, and D–R parameters for adsorption isotherm of strontium on AC/Fe_2O_3 at 25°C with R^2 values corresponding to linear fitting of the data

	Langumir parameter		
	X_m	K	R^2
AC/1% Fe_2O_3	0.153	7.092	0.92
AC/10% Fe_2O_3	1.39	6.172	0.92
	Freundlich parameter		
	K_f	1/n	R^2
AC/1% Fe_2O_3	21605	0.23	0.95
AC/10% Fe_2O_3	687	1.078	0.94
	D–R parameter		
	Q_m	B	R^2
AC/1% Fe_2O_3	8287	0.00095	0.95
AC/10% Fe_2O_3	254	0.00035	0.98

Table 4
Maximum sorption capacity of various adsorbents for Sr(II)

Material	Adsorption capacity (mg/g)	Reference
Dolomite powder	1.17	[29]
Natural clinoptilolite	9.8	[31]
Sericite	1.6	[32]
Magnetic Fe_2O_3 modified sawdust	12.59	[19]
Zeolite A	99	[33]
Fe_2O_3 modified activated carbon	10.1	Present study

The mean free energy (E) of the adsorption process between strontium and the AC composites are found using a D-R isotherm. The mean sorption energy for adsorption of strontium ion on AC with 1 and 10 wt.% Fe_2O_3 loading was calculated to be 16.23 kJ/mol and 26 kJ/mol, respectively. These result suggests that adsorption of strontium ion on surface of AC composites are chemisorption process for both cases. The results suggest that the adsorption binding energy increases with Fe_2O_3 loading.

The calculated adsorption capacity for AC with 1 and 10 wt.% Fe_2O_3 loading in this study was found to be around 9.1 and 10.1 mg/g which is one of the highest among the previously reported materials for removal of strontium from water (Table 4). This finding indicates that the presence of Fe_2O_3 with high surface area significantly enhanced the adsorption capacity of AC and efficiency of Sr removal.

4. Conclusion

Surface modification of AC with Fe_2O_3 nanoparticles showed effective removal of strontium from water. Loading of Fe_2O_3 nanoparticles significantly improved the surface

area of AC which facilitated the adsorption of strontium ions. The optimum values of the operating parameters for maximum strontium removal were found at: adsorbent dosage of 150 mg, pH of 7, contact time of 150 min, and agitation speed of 400 rpm for AC with 1 and 10 wt.% Fe_2O_3 nanoparticle loading. High adsorption of strontium of 93% and 100% for AC with 1and 10 wt.% Fe_2O_3 nanoparticle loading, respectively, were achieved. These data indicate that synthesised AC-Fe_2O_3 composites based on a cheap AC material might be efficiently used for produced water pretreatment and desalination pre-treatment for strontium removal.

Acknowledgment

The authors are grateful to the Qatar Environment and Energy Research Institute (QEERI), Hamad Bin Khalifa University (HBKU), Qatar Foundation for the financial support.

References

[1] T. Annunciado, T. Sydenstricker, S. Amico, Experimental investigation of various vegetable fibers as sorbent materials for oil spills, Marine Pollut. Bull., 50 (2005) 1340–1346.
[2] A. Fakhru'l-Razi, A. Pendashteh, L.C. Abdullah, D.R.A. Biak, S.S. Madaeni, Z.Z. Abidin, Review of technologies for oil and gas produced water treatment, J. Hazard. Mater., 170 (2009) 530–551.
[3] A.K. Fard, T. Rhadfi, G. Mckay, M. Al-marri, A. Abdala, N. Hilal, M.A. Hussien, Enhancing oil removal from water using ferric oxide nanoparticles doped carbon nanotubes adsorbents, Chem. Eng. J., 293 (2016) 90–101.
[4] J.A. Veil, M.G. Puder, D. Elcock, R.J. Redweik Jr, A white paper describing produced water from production of crude oil, natural gas, and coal bed methane, Argonne National Laboratory, Technical Report, 2004.
[5] B. Hansen, S. Davies, Review of potential technologies for the removal of dissolved components from produced water, Chem. Eng. Res. Design, 72 (1994) 176–188.
[6] V. Pacary, Y. Barré, E. Plasari, Method for the prediction of nuclear waste solution decontamination by coprecipitation of strontium ions with barium sulphate using the experimental data obtained in non-radioactive environment, Chem. Eng. Res. Design, 88 (2010) 1142–1147.
[7] A.Y. Zhang, T. Akashi, B.P. Zhang, T. Goto, Electrical conductivity of partially ion exchanged Sr and Ba β-alumina single crystals determined by ac impedance spectroscopy, Mater. Lett., 60 (2006) 2834–2836.
[8] A. Zhang, C. Chen, E. Kuraoka, M. Kumagai, Impregnation synthesis of a novel macroporous silica-based crown ether polymeric material modified by 1-dodecanol and its adsorption for strontium and some coexistent metals, Sep. Purif. Technol., 62 (2008) 407–414.
[9] A.K. Fard, G. Mckay, Y. Manawi, Z. Malaibari, M.A. Hussien, Outstanding adsorption performance of high aspect ratio and super-hydrophobic carbon nanotubes for oil removal, Chemosphere, 164 (2016) 142–155.
[10] S. Rao, B. Paul, K. Lal, S. Narasimhan, J. Ahmed, Effective removal of cesium and strontium from radioactive wastes using chemical treatment followed by ultra filtration, J. Radioanal. Nucl. Chem., 246 (2000) 413–418.
[11] A.K. Fard, T. Rhadfi, M. Khraisheh, M.A. Atieh, M. Khraisheh, N. Hilal, Reducing flux decline and fouling of direct contact membrane distillation by utilizing thermal brine from MSF desalination plant, Desalination, 379 (2016) 172–181.
[12] A.K. Fard, Y.M. Manawi, T. Rhadfi, K.A. Mahmoud, M. Khraisheh, F. Benyahia, Synoptic analysis of direct contact membrane distillation performance in Qatar: a case study, Desalination, 360 (2015) 97–107.
[13] S. Chegrouche, A. Mellah, M. Barkat, Removal of strontium from aqueous solutions by adsorption onto activated carbon: kinetic and thermodynamic studies, Desalination, 235 (2009) 306–318.
[14] R.A. Shawabkeh, D.A. Rockstraw, R.K. Bhada, Copper and strontium adsorption by a novel carbon material manufactured from pecan shells, Carbon, 40 (2002) 781–786.
[15] E. Başçetin, G.l. Atun, Adsorptive removal of strontium by binary mineral mixtures of montmorillonite and zeolite, J. Chem. Eng. Data, 55 (2009) 783–788.
[16] A. Ahmadpour, M. Zabihi, M. Tahmasbi, T.R. Bastami, Effect of adsorbents and chemical treatments on the removal of strontium from aqueous solutions, J. Hazard. Mater., 182 (2010) 552–556.
[17] S.M. Hasany, M.H. Chaudhary, Adsorption studies of strontium on manganese dioxide from aqueous solutions, Int. J. Appl. Rad. Isotop., 32 (1981) 899–904.
[18] T. Cole, G. Bidoglio, M. Soupioni, M. O'Gorman, N. Gibson, Diffusion mechanisms of multiple strontium species in clay, Geochim. Cosmochim. Acta, 64 (2000) 385–396.
[19] Z. Cheng, Z. Gao, W. Ma, Q. Sun, B. Wang, X. Wang, Preparation of magnetic Fe_3O_4 particles modified sawdust as the adsorbent to remove strontium ions, Chem. Eng. J., 209 (2012) 451–457.
[20] N. Sahai, S.A. Carroll, S. Roberts, P.A. O'Day, X-ray absorption spectroscopy of strontium (II) coordination: II. Sorption and precipitation at kaolinite, amorphous silica, and goethite surfaces, J. Colloid Interf. Sci., 222 (2000) 198–212.
[21] O.N. Karasyova, L.I. Ivanova, L.Z. Lakshtanov, L. Lövgren, Strontium sorption on hematite at elevated temperatures. J. Colloid Interf. Sci., 220 (1999) 419–428.
[22] T.-J. Liang, C.-N. Hsu, D.-C. Liou, Modified Freundlich sorption of cesium and strontium on Wyoming bentonite, Appl. Rad. Isotop., 44 (1993) 1205–1208.
[23] C.H. Jeong, Mineralogical and hydrochemical effects on adsorption removal of cesium-137 and strontium-90 by kaolinite, J. Environ. Sci. Health, Part A, 36 (2001) 1089–1099.
[24] A. Günay, E. Arslankaya, I. Tosun, Lead removal from aqueous solution by natural and pretreated clinoptilolite: adsorption equilibrium and kinetics, J. Hazard. Mater., 146 (2007) 362–371.
[25] M. Dubinin, The potential theory of adsorption of gases and vapors for adsorbents with energetically nonuniform surfaces, Chem. Rev., 60 (1960) 235–241.
[26] A. Youssef, S.M. EL-Khouly, T. El-Nabarawy, Removal of Pb (II) and Cd (II) from aqueous solution using oxidized activated carbons developed from pecan shells, Carbon Lett., 9 (2008) 8–16.
[27] H. Yuh-Shan, Citation review of Lagergren kinetic rate equation on adsorption reactions, Scientometrics, 59 (2004) 171–177.
[28] Y.-S. Ho, G. McKay, Pseudo-second order model for sorption processes, Process Biochem., 34 (1999) 451–465.
[29] A. Ghaemi, M. Torab-Mostaedi, M. Ghannadi-Maragheh, Characterizations of strontium (II) and barium (II) adsorption from aqueous solutions using dolomite powder, J. Hazard. Mater., 190 (2011) 916–921.
[30] Collins, I.R., Surface electrical properties of barium sulfate modified by adsorption of poly α, β aspartic acid, J. Colloid Interf. Sci., 212 (1999) 535–544.
[31] I. Smičiklas, S. Dimović, I. Plećaš, Removal of Cs^+, Sr^{2+} and Co^{2+} from aqueous solutions by adsorption on natural clinoptilolite, Appl. Clay Sci., 35 (2007) 139–144.
[32] D. Tiwari, S.-M. Lee, Physico-chemical studies in the removal of Sr (II) from aqueous solutions using activated sericite, J. Environ. Radioact., 147 (2015) 76–84.
[33] H. Faghihian, M. Moayed, A. Firooz, M. Iravani, Evaluation of a new magnetic zeolite composite for removal of Cs^+ and Sr^{2+} from aqueous solutions: kinetic, equilibrium and thermodynamic studies, Comptes Rendus Chimie, 17 (2014) 108–117.